Change of Fermi surface states related with two different T_c-raising mechanisms in iron pnictide superconductors

A. Takemori,[1] T. Hajiri,[2] S. Miyasaka,[1] Z. H. Tin,[1] T. Adachi,[1] S. Ideta,[3,4] K. Tanaka,[3,4] M. Matsunami,[3,4] and S. Tajima[1]

[1]*Department of Physics, Osaka University, Osaka 560-0043, Japan*

[2]*Department of Materials Physics, Graduate School of Engineering, Nagoya University, Nagoya 464-8603, Japan*

[3]*UVSOR Facility, Institute for Molecular Science, Okazaki 444-8585, Japan*

[4]*School of Physical Sciences, The Graduate University for Advanced Studies (SOKENDAI), Okazaki 444-8585, Japan*

The evolution of Fermi surface (FS) states of $NdFeAs_{1-x}P_xO_{0.9}F_{0.1}$ single crystals with As/P substitution has been investigated. The critical temperature T_c and the power-law exponent (n) of temperature-dependent resistivity [$\rho(T) = \rho_0 + AT^n$] show a clear correlation above $x = 0.2$, suggesting that T_c is enhanced with increasing bosonic fluctuations in the same type of FS state. Around $x = 0.2$, all the transport properties show anomalies, indicating that $x \sim 0.2$ is the critical composition of a drastic FS change. Angle-resolved photoemission spectroscopy has more directly revealed the distinct change of FS around $x = 0.2$, that one hole FS disappears at the Brillouin zone center and the other FS with a propellerlike shape appears at the zone corner with decreasing x. These results are indicative of the existence of two types of FS states with different nesting conditions that are related with two T_c-raising mechanisms in this system.

Since the discovery of iron-based superconductors (IBSs), many experimental and theoretical studies have been performed [1,2], but the superconducting (SC) mechanism of this system has not yet been clarified. The IBSs are multiband systems with several two-dimensional Fermi surfaces (FSs). It has been theoretically predicted that spin or orbital fluctuations play an important role in the pairing mechanism, but this issue is still under debate [3–5]. Experimentally, the empirical relation between T_c and the local structural parameter has been reported [6,7]. This was explained by the theory of Kuroki *et al.* where the local structural parameters have a close relation to the electronic band structure and FS states [4,8]. However, there is no distinct experimental evidence for their relation. In addition, the FS topology of IBSs has a strongly material dependence [9–17], which causes difficulties in clarifying the SC mechanism of IBSs from the viewpoints of FS topology and related nesting conditions. Therefore, to understand the SC mechanism of IBSs, it is necessary to study experimentally the change of FS states related with the nesting condition and pairing mechanism in adequate systems, where the local structural parameters and FS states can be systematically controlled.

$RFeAs_{1-x}P_xO_{1-y}F_y$ (R = La or rare-earth element) is a good platform for such a study. There are several advantages. First, isovalent As/P substitution induces a large and systematic change of the crystal structure including the local $Fe(As/P)_4$ tetrahedron without any modification of the band filling [18–22]. The deformation of the local $Fe(As/P)_4$ tetrahedron is expected to seriously affect the FS topology [4]. Second, we can cover a wide range of T_c from ~ 0 to ~ 50 K using several R systems [18]. Third, the strength of the antiferromagnetic (AF) correlation can be systematically changed by varying x [23].

In previous studies, we have reported the transport properties in polycrystalline samples of 1111-type $RFeAs_{1-x}P_xO_{1-y}(F/H)_y$ (R = La, Pr, and Nd) [18–20]. In the La-1111 system, three SC regions exist near three different AF phases. In the low electron doping region of $y \sim 0.1$, these systems show a crossover behavior between two different SC states by As/P substitution. Our investigation has indicated that $RFeAs_{1-x}P_xO_{1-y}F_y$ with a F concentration of $y \sim 0.1$ has two different T_c-raising mechanisms, related to two different FS states and nesting conditions around $x = 0$ and above $x = 0.2$–0.4 [18–20,23]. In the present Rapid Communication, to clarify the x-dependent change of electronic structures and FS topology directly, we have investigated the transport properties and angle-resolved photoemission spectroscopy (ARPES) using single crystals of $NdFeAs_{1-x}P_xO_{0.9}F_{0.1}$.

Single crystals of $NdFeAs_{1-x}P_xO_{0.9}F_{0.1}$ with $x = 0$–1.0 were grown from a mixture of NdAs, NdP, Fe_2O_3, Fe, and FeF_2 under a high pressure of 3.8 GPa by using a cubic anvil press machine. It was heated up to ~ 1400 °C, kept for 12 h, and then slowly cooled down to ~ 800 °C for 72 h. The typical size of the single crystal was about $1 \times 1 \times 0.03$ mm^3 [24]. Here, we use a nominal P and F concentration as x and y (=0.1). The actual F concentration estimated by the electron probe microanalyzer was approximately 0.05 in the whole x region. The P content x determined by energy dispersive x-ray spectroscopy was nearly the same as the nominal one.

The magnetic susceptibility was measured in a magnetic field of 10 Oe, and the samples with $x \leqq 0.8$ show a diamagnetic behavior below T_c. The temperature (T) dependence of in-plane electrical resistivity $\rho(T)$ was measured by a standard four-probe method. The Hall coefficient R_H was measured in magnetic fields parallel to the c axis up to 7 T. The ARPES measurements were carried
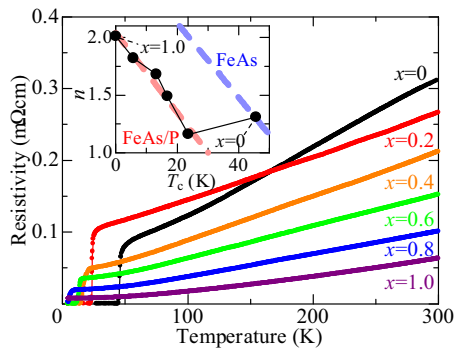
FIG. 1. T dependence of in-plane resistivity $\rho(T)$ for NdFeAs$_{1-x}$P$_x$O$_{0.9}$F$_{0.1}$ single crystals with $x = 0$–1.0. The inset shows the relation between T_c and the power n of T in $\rho(T)$. The red and blue dashed lines represent the two different correlations between T_c and n in RFeAs$_{1-x}$P$_x$O$_{0.9}$F$_{0.1}$ ($x > 0.2$–0.4) and RFeAsO$_{1-y}$F$_y$/RFeAsO$_{1-y}$ (R = La, Pr, and Nd) [18].

out at BL-5U and 7U of UVSOR Facility at Institute for Molecular Science [25]. The k_z dependence of FS topology has been investigated by ARPES with various incident photon energies. It has been confirmed that the topology of the observed FSs has been almost unchanged along the k_z direction. Here, the in-plane ARPES measurements have been performed using incident photons with $h\nu = 36$ eV polarized linearly. The MBS A-1 analyzer was used with an energy resolution of $\sim$15 meV. The angular resolution was $\sim$0.17°. The single crystals were cleaved at $\sim$12 K in an ultrahigh vacuum ($\sim 1 \times 10^{-10}$ Torr). The Fermi level (E_F) was calibrated using an evaporated gold film.

Figure 1 shows $\rho(T)$ for single crystals of NdFeAs$_{1-x}$P$_x$O$_{0.9}$F$_{0.1}$ with $x = 0$–1.0. The T and x dependences of the in-plane resistivity for single crystals are very similar to those of polycrystalline samples [18]. The room-T resistivity decreases with x. The samples below $x = 0.8$ show a SC transition, and T_c determined as zero resistivity T is almost the same as the onset T of the diamagnetism of magnetic susceptibility. On the other hand, $\rho(T)$ shows no anomaly due to the spin density wave (SDW) transition in the whole x region. $\rho(T)$ can be expressed as $\rho(T) = \rho_0 + AT^n$ at low T, where ρ_0 is the residual resistivity, n the power-law exponent of T, and A the coefficient. The fitting of $\rho(T)$ was performed between the onset T of the resistive transition and 100 K. The x dependences of T_c, n, ρ_0, and A are presented in Fig. 2. NdFePO$_{0.9}$F$_{0.1}$ ($x = 1.0$) does not undergo a SC transition and $\rho(T)$ shows T^2 behavior, indicating that the system is a conventional Fermi liquid without any bosonic fluctuation. With decreasing x, T_c gradually increases up to $\sim$25 K, and n systematically decreases and becomes close to unity at $x \sim 0.2$. Below $x = 0.2$, T_c is rapidly enhanced and n is slightly increased.

The x dependence of T_c and n has a clear relation in the composition region between $x = 0.2$ and 1.0. The inset of Fig. 1 represents the T_c vs n plot for the present single crystals. The figure also shows the two T_c-n relationships, which have been clarified by previous studies in polycrystalline samples [18,26]. Above $x = 0.2$, T_c and n follow one of the linear T_c-n relationships, as shown by the red dashed line in the
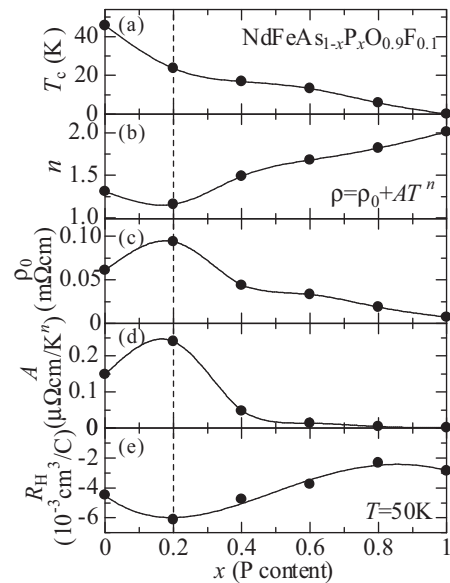

FIG. 2. x dependence of physical properties for NdFeAs$_{1-x}$P$_x$O$_{0.9}$F$_{0.1}$ single crystals. (a) T_c. (b) Power n of T in $\rho(T) = \rho_0 + AT^n$. (c) Residual resistivity ρ_0. (d) The coefficient A. (e) R_H at 50 K. Solid lines are guide for the eyes. The dashed vertical line indicates a critical concentration of $x = 0.2$.

inset of Fig. 1. This result indicates that the nesting between the hole and electron FSs becomes better with decreasing x, which gives a stronger bosonic fluctuation as monitored by the power n, and results in the enhancement of T_c. On the other hand, the data point of T_c and n for NdFeAsO$_{0.9}$F$_{0.1}$ ($x = 0$) is located on the other T_c-n scaling line. This reveals that the FS topology and the nesting conditions are quite different between the composition regions at $x < 0.2$ and $x > 0.2$, and $x \sim 0.2$ is the critical concentration for the change of FS as well as the related bosonic fluctuations. As shown in Fig. 2(e), the x-dependent R_H at 50 K shows a broad minimum around $x = 0.2$, suggesting the critical change of the electronic structure, too.

Recent experimental investigations of transports and NMR have indicated that the LaFeAs$_{1-x}$P$_x$O has two different AF states around $x = 0$ and 0.6, suggesting the change of the FS state and the related nesting condition by the As/P solid solution [19,27,28]. These AF orders are suppressed by F doping, and T_c shows a double-peak structure at $x = 0$ and 0.6 in LaFeAs$_{1-x}$P$_x$O$_{1-y}$F$_y$ with $y = 0.05$ [19]. With further F substitution, these peaks of T_c merge and create a single peak around $x = 0.4$ in the $y = 0.1$ system [18,20]. In LaFeAs$_{1-x}$P$_x$O$_{1-y}$F$_y$ with $y = 0.05$ and 0.1, n of $\rho(T)$ is systematically decreased from 2 to about 1, when x decreases down to $x \sim 0.6$ and 0.4, respectively. These results are suggestive of the enhancement of bosonic fluctuation such as an AF fluctuation. NMR studies in LaFeAs$_{1-x}$P$_x$O$_{1-y}$F$_y$ have revealed that $(T_1T)^{-1}$ shows a distinct enhancement around $(x, y) = (0.6, 0.05)$ and $(0.4, 0.1)$, that also indicates the existence of a strong AF fluctuation [23,29]. In the present NdFeAs$_{1-x}$P$_x$O$_{0.9}$F$_{0.1}$, the power n of $\rho(T)$ also shows similar behavior to the La system, indicating the existence of a strong AF fluctuation around $x = 0.2$.
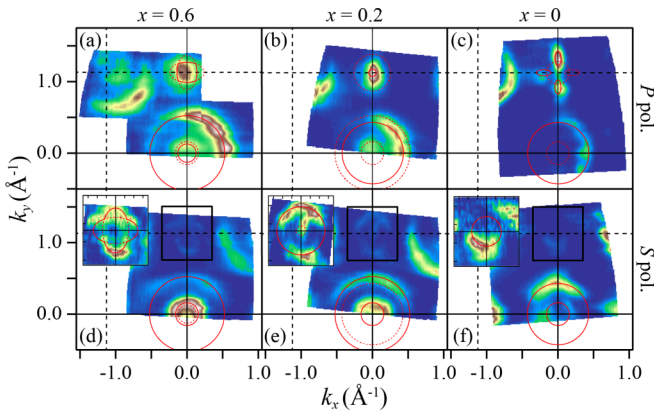
FIG. 3. In-plane FS mapping of NdFeAs$_{1-x}$P$_x$O$_{0.9}$F$_{0.1}$ single crystals with $x = 0.6$ [(a), (d)], 0.2 [(b), (e)], and 0 [(c), (f)], respectively. The upper [(a)–(c)] and lower [(d)–(f)] panels show the results in P and S geometries, respectively. Insets of (d)–(f) show the results around the BZ corner by using different color gradations. The solid lines indicate the FSs observed in the polarization geometry, while the dashed ones are the FSs observed in the other geometry.

FIG. 4. ARPES intensity mapping in the P polarization geometry for NdFeAs$_{1-x}$P$_x$O$_{0.9}$F$_{0.1}$ single crystals with $x = 0.6$ [(a), (e)], 0.2 [(b), (f)], and 0 [(c), (g)]. (a)–(c) and (e)–(g) show the results of the energy-momentum cut around the BZ center $(0, 0)$ and around the corner $(0, \pi)$, respectively. Solid lines indicated the band dispersion estimated from anomalies such as peaks and kinks in EDCs at various k_x and in momentum distribution curves (MDCs) at various binding energies. The band dispersions should be symmetric with respect to the line at $k_x = 0$ because of the crystal symmetry, but some parts of the band dispersion indicated by the dashed lines cannot be estimated from the EDCs and MDCs due to the low ARPES intensity. In order to draw these band dispersions, several previous works have been referred [9,11,12,35]. (d) and (h) show the EDCs of $x = 0$, 0.2, and 0.6 at the BZ center and corner ($k_x = 0$), respectively. The bars indicate the energy position of the top or the bottom of the bands shown in (a)–(c) and (e)–(g). In (d), the triangles indicate the energy position of the top of the xz band.

As shown in Fig. 2, ρ_0 and A are clearly enhanced around $x = 0.2$. These behaviors cannot be explained by the conventional spin fluctuation theory, but they suggest the existence of additional bosonic fluctuations. The similar anomalies together with T-linear $\rho(T)$ were observed near the quantum critical point (QCP) in heavy fermion Ce compounds [30–33]. These heavy fermion systems have maximum T_c values and show anomalies of ρ_0 and A at critical pressures (P) of the valence transition of the Ce ion, which is apart from magnetic QCP in the P-T phase diagram. In NdFeAs$_{1-x}$P$_x$O$_{0.9}$F$_{0.1}$, isovalent As/P substitution does not cause the change of the Fe $3d$ band filling, but induces the distinct change of the electronic structure near E_F as described later, and concomitantly the charge fluctuation at a critical concentration $x \sim 0.2$, which could enhance T_c at $x \sim 0.2$.

This change of electronic structure at a critical concentration of $x \sim 0.2$ has been directly observed by ARPES measurement. Figure 3 shows the in-plane FS mapping for $x = 0.6$, 0.2, and 0 at ~ 12 K. Here, x and y axes are parallel to the Fe-Fe bond direction within the plane. In the P (S) polarization geometry, the electric field vector of incident photons is parallel (perpendicular) to the mirror plane defined by the analyzer slit parallel to the x axis and the normal vector (z axis) of the cleaved sample surface. The propagator vectors of the incident photons are located in the mirror plane (xz plane) [25]. In the present ARPES measurements, the x axis is not perfectly parallel to the analyzer slit, but the misalignment angle is less than $\sim 6°$. In Fig. 3, the photoemission intensity has been integrated over the energy range of $E_F \pm 5$ meV.

The FSs with xz, $3z^2 - r^2$, and $x^2 - y^2$ characters of the Fe $3d$ orbital can be detected in the P polarization geometry, while those with yz and xy in the S polarization around the Brillouin zone (BZ) center [34,35]. First, we focus our discussion on the data for the BZ center. As is seen in Figs. 3(a) and 3(d), the two small FSs observed in the P and S polarization geometries have a quite similar size, indicating that the bands related with these FSs are almost degenerate
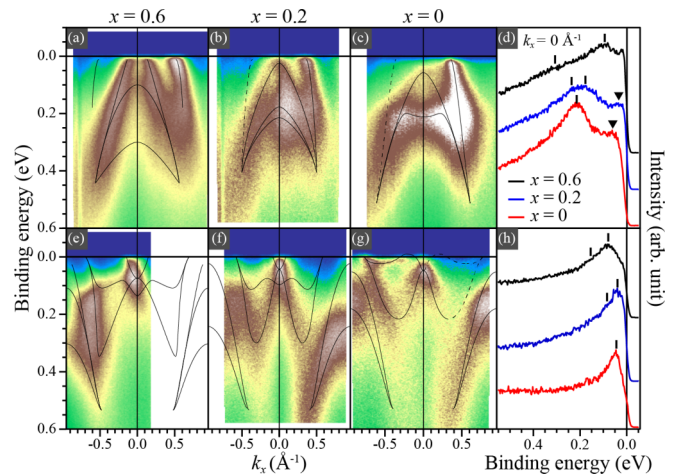
near the BZ center $(0, 0)$ for $x = 0.6$. Therefore, the orbital characters of these FSs have been assigned to xz and yz. This assignment is consistent with previous theoretical and experimental studies in the related iron-phosphorous material, LaFePO [4,9–11,36]. In the 1111 system, there are other theoretically predicted electronic bands with xy and $3z^2 - r^2$ characters near the BZ center [4,36]. The outer FS observed in the P polarization geometry may have a $3z^2 - r^2$ character. As seen in Figs. 3(a) and 4(a), however, the FS size is larger and the energy level of the related band is higher than those predicted by the theoretical studies [4,36]. The orbital character of the outer FS is unclear at present. In addition, previous ARPES studies indicated that 1111-type compounds suffer from a polar surface problem [12,37]. Due to the lack of a charge neutral cleavage plane, the doping level of the cleaved surface is significantly different from the nominal doping level expected from the chemical composition. This outer FS might be originated from the surface electronic state. Therefore, we discuss here only the inner FSs, which show a systematic change with the P content (x), suggesting a change of the bulk electronic state.

As shown in Fig. 3, large and small FSs were observed around the BZ center also in the $x = 0.2$ and 0 samples. The small FS with an xz character observed in the P polarization geometry disappears below $x = 0.2$ [Figs. 3(a)–3(c)], while the FSs with a yz character in the S geometry are almost

unchanged with a decrease of x [Figs. 3(d)–3(f)]. The disappearance of the xz FS below $x = 0.2$ can be seen also in the band dispersion. Figure 4 illustrates the ARPES intensity mapping that corresponds to the band dispersion on the P polarization geometry for $x = 0.6$, 0.2, and 0. As shown in Figs. 4(a)–4(c), the energy level of the inner xz band in the P geometry decreases with decreasing x. The top of the xz band touches E_F at $x \sim 0.2$ [Fig. 4(b)], and this band sinks down perfectly below E_F at $x \sim 0$. This x dependence of the bands can be also seen in the energy distribution curves (EDCs) in Fig. 4(d). Resultantly, the xz FS around the BZ center disappears below $x \sim 0.2$, indicating the change of the FS states and the related nesting condition at this critical x.

Previous ARPES studies have indicated that LaFePO has doubly degenerate small hole FSs around the BZ center, while the 1111-type FeAs compounds have only one small FS [9–12]. The present study has clarified the missing link of the FS state between 1111-type FeP and FeAs compounds. In this system, As/P substitution induces the change of the electronic structure concomitantly with a monotonic transformation of the local structural parameters around the Fe ion [20–22]. Particularly, the bond angle of As/P-Fe-As/P shows the linear x dependence from $\sim 111°$ for $x = 0$ to $\sim 118°$ for $x = 1.0$ in NdFeAs$_{1-x}$P$_x$O$_{0.9}$F$_{0.1}$, which have been determined by our structural analysis for the polycrystalline samples using synchrotron x-ray diffraction. The present ARPES results clearly demonstrate that the systematic change of the local structure directly affects the FS state and band structure near the BZ center, particularly the xz hole band and its FS. The band calculation, where the As-Fe-As bond angle is virtually changed, has demonstrated a similar FS change and xz/yz band splitting near the Γ point with a decreasing bond angle down to $\sim 109°$ [38,39]. According to the calculation, xz/yz band splitting is accompanied by a lifting of the energy level of the xy band up to E_F, which has been observed in our preliminary ARPES experiments.

Next, we see the FSs around the BZ corner $(0, \pi)$ in Fig. 3. Since the photoemission intensity near E_F is low around the BZ corner in the S polarization geometry, the results are presented by different color gradations in the insets of Figs. 3(d)–3(f). At $x = 0.6$, two FSs with an elliptical shape exist around the BZ corner [Figs. 3(a) and 3(d)]. The FS shape around the BZ corner drastically changes with decreasing x. At $x = 0.2$, there are two cylindrical FSs, while the FS for $x = 0$ has quite different shapes, namely, one is cylindrical and the other is propellerlike.

As shown in Fig. 4, the band dispersion around the BZ corner is complicated and its x dependence is nonmonotonic. In the P geometry of the $x = 0.6$ and 0.2 samples, one electron band is observed around the BZ corner, and it creates elliptical and cylindrical FSs, respectively. On the other hand, there are two other bands with complicated dispersions around the binding energy range of 0–0.3 eV. As shown in Figs. 4(e)–4(h), all the bands tend to lift up with decreasing x. For $x = 0$, the bottom of the electron band with parabolic dispersion shifts up above E_F and this electron FS disappears. One of the other bands, located around the binding energy of ~ 0.1 eV for $x = 0.6$ and 0.2, shows a relatively large energy shift between $x = 0.2$ and 0 [Fig. 4(h)]. At $x = 0$, this band crosses E_F and makes propellerlike hole FSs, which have

been observed in other 1111-type pure As systems [11,12]. The surface electronic state may affect some of the FSs and the bands around the BZ corner [12,37], but the observed x dependence is essentially originating from the change of the bulk electronic state.

The discontinuous change of band dispersion and FSs between $x = 0.2$ and 0 induces the change of the nesting condition and the different bosonic fluctuations. As a result, it causes a different T_c-raising mechanism below and above $x \sim 0.2$. Above $x \sim 0.2$, two cylindrical hole FSs around the BZ center and two electronic FSs with an almost cylindrical shape around the zone corner have a good nesting condition, which produces a strong spin fluctuation. The good FS nesting in the P-doping region has been theoretically predicted by Usui *et al.* [40], and the enhancement of the low-energy spin fluctuation at $x \sim 0.2$ has been observed by the present study of $\rho(T)$ and also by a previous NMR study in La-1111 systems [23]. This spin fluctuation regime does not remain below $x \sim 0.2$ because one hole FS disappears and the FS topology around the BZ corner becomes complicated, giving a moderate nesting condition. At $x \sim 0$, the xy hole band exists very near E_F around the BZ center, which suggests some other types of bosonic fluctuations. First, this band and FSs around the BZ corner may induce a spin fluctuation with a relatively higher energy. In fact, previous results of an NMR study suggested the existence of a spin fluctuation with a higher energy [23]. Second, the xy band near E_F may also induce some charge fluctuation. These spin or charge fluctuations could be another candidate for bosonic fluctuations related with the SC mechanism in the 1111-type FeAs system.

In summary, transport and ARPES studies have been performed using NdFeAs$_{1-x}$P$_x$O$_{0.9}$F$_{0.1}$ single crystals to clarify the x dependence of the bosonic fluctuation and electronic bands that should be related with the SC mechanism. In the present system, T_c gradually increases from 0 to ~ 25 K with decreasing x from $x = 1.0$ to 0.2, and is rapidly enhanced below $x = 0.2$. At $0.2 \leqq x \leqq 1.0$, T_c increases and the T dependence of $\rho(T)$ changes from T^2 to T-linear behavior monotonously with decreasing x. This close correlation of T_c and $\rho(T)$ implies that T_c is enhanced with increasing bosonic fluctuation with the same FS topology. On the other hand, T_c and the T dependence of $\rho(T)$ have a different relationship below $x \sim 0.2$. The slope of $\rho(T)$, the residual resistivity, and R_H have anomalies around $x = 0.2$. These results indicate that the FS and related bosonic fluctuations drastically change at $x \sim 0.2$, which is consistent with the ARPES observation of a clear change of FS around $x = 0.2$. The hole FS with an xz orbital character around the BZ center disappears at $x \sim 0.2$ with decreasing x. Around the BZ corner, the FS shape is clearly changed between $x = 0.2$ and 0. The significant variation of FSs around $x = 0.2$ must induce the change of bosonic fluctuations and resultantly causes a further enhancement of T_c below $x \sim 0.2$ in As/P solid solution 1111 systems.

[1] Y. Kamihara, T. Watanabe, M. Hirano, and H. Hosono, J. Am. Chem. Soc. **130**, 3296 (2008).

[2] H. Hosono and K. Kuroki, Physica C **514**, 399 (2015).

[3] I. I. Mazin, D. J. Singh, M. D. Johannes, and M. H. Du, Phys. Rev. Lett. **101**, 057003 (2008).

[4] K. Kuroki, H. Usui, S. Onari, R. Arita, and H. Aoki, Phys. Rev. B **79**, 224511 (2009).

[5] H. Kontani and S. Onari, Phys. Rev. Lett. **104**, 157001 (2010).

[6] Y. Mizuguchi, Y. Hara, K. Deguchi, S. Tsuda, T. Yamaguchi, K. Takeda, H. Kotegawa, H. Tou, and Y. Takano, Supercond. Sci. Technol. **23**, 054013 (2010).

[7] C.-H. Lee, A. Iyo, H. Eisaki, H. Kito, M. T. Fernandez-Diaz, T. Ito, K. Kihou, H. Matsuhata, M. Braden, and K. Yamada, J. Phys. Soc. Jpn. **77**, 083704 (2008).

[8] In this Rapid Communication, "FS states" means electronic states with characteristic FSs observed in IBSs. For example, the theoretical study by Kuroki *et al.* at an early stage has predicted that one of the 1111-type IBSs, the NdFeAsO system, has several two-dimensional hole and electron FSs including the xy hole FS, while the xy hole FS disappears in the related material LaFePO [4]. In other words, their investigation has theoretically demonstrated that these 1111-type systems have different FS states.

[9] D. H. Lu, M. Yi, S.-K. Mo, A. S. Erickson, J. Analytis, J.-H. Chu, D. J. Singh, Z. Hussain, T. H. Geballe, I. R. Fisher, and Z.-X. Shen, Nature (London) **455**, 81 (2008).

[10] D. H. Lu, M. Yi, S.-K. Mo, J. G. Analytis, J.-H. Chu, A. S. Erickson, D. J. Singh, Z. Hussain, T. H. Geballe, I. R. Fisher, and Z.-X. Shen, Physica C **469**, 452 (2009).

[11] I. Nishi, M. Ishikado, S. Ideta, W. Malaeb, T. Yoshida, A. Fujimori, Y. Kotani, M. Kubota, K. Ono, M. Yi, D. H. Lu, R. Moore, Z.-X. Shen, A. Iyo, K. Kihou, H. Kito, H. Eisaki, S. Shamoto, and R. Arita, Phys. Rev. B **84**, 014504 (2011).

[12] A. Charnukha, S. Thirupathaiah, V. B. Zabolotnyy, B. Büchner, N. D. Zhigadlo, B. Batlogg, A. N. Yaresko, and S. V. Borisenko, Sci. Rep. **5**, 10392 (2015).

[13] D. V. Evtushinsky, D. S. Inosov, V. B. Zabolotnyy, A. Koitzsch, M. Knupfer, B. Büchner, M. S. Viazovska, G. L. Sun, V. Hinkov, A. V. Boris, C. T. Lin, B. Keimer, A. Varykhalov, A. A. Kordyuk, and S. V. Borisenko, Phys. Rev. B **79**, 054517 (2009).

[14] W. Malaeb, T. Shimojima, Y. Ishida, K. Okazaki, Y. Ota, K. Ohgushi, K. Kihou, T. Saito, C. H. Lee, S. Ishida, M. Nakajima, S. Uchida, H. Fukazawa, Y. Kohori, A. Iyo, H. Eisaki, C.-T. Chen, S. Watanabe, H. Ikeda, and S. Shin, Phys. Rev. B **86**, 165117 (2012).

[15] T. Yoshida, I. Nishi, S. Ideta, A. Fujimori, M. Kubota, K. Ono, S. Kasahara, T. Shibauchi, T. Terashima, Y. Matsuda, H. Ikeda, and R. Arita, Phys. Rev. Lett. **106**, 117001 (2011).

[16] H. Suzuki, T. Kobayashi, S. Miyasaka, T. Yoshida, K. Okazaki, L. C. C. Ambolode, S. Ideta, M. Yi, M. Hashimoto, D. H. Lu, Z.-X. Shen, K. Ono, H. Kumigashira, S. Tajima, and A. Fujimori, Phys. Rev. B **89**, 184513 (2014).

[17] S. V. Borisenko, V. B. Zabolotnyy, D. V. Evtushinsky, T. K. Kim, I. V. Morozov, A. N. Yaresko, A. A. Kordyuk, G. Behr, A. Vasiliev, R. Follath, and B. Buchner, Phys. Rev. Lett. **105**, 067002 (2010).

[18] S. Miyasaka, A. Takemori, T. Kobayashi, S. Suzuki, S. Saijo, and S. Tajima, J. Phys. Soc. Jpn. **82**, 124706 (2013).

[19] K. T. Lai, A. Takemori, S. Miyasaka, F. Engetsu, H. Mukuda, and S. Tajima, Phys. Rev. B **90**, 064504 (2014).

[20] S. Miyasaka, M. Uekubo, H. Tsuji, M. Nakajima, S. Tajima, T. Shiota, H. Mukuda, H. Sagayama, H. Nakao, R. Kumai, and Y. Murakami, Phys. Rev. B **95**, 214515 (2017).

[21] K. T. Lai, A. Takemori, S. Miyaska, S. Tajima, A. Nakao, H. Nakao, R. Kumai, and Y. Murakami, JPS Conf. Proc. **1**, 012104 (2014).

[22] A. Takemori, S. Saijo, S. Suzuki, S. Miyasaka, S. Tajima, A. Nakao, H. Nakao, R. Kumai, and Y. Murakami, J. Phys. Soc. Jpn. Suppl. B **81**, SB043 (2012).

[23] T. Shiota, H. Mukuda, M. Uekubo, F. Engetsu, M. Yashima, Y. Kitaoka, K. T. Lai, H. Usui, K. Kuroki, S. Miyasaka, and S. Tajima, J. Phys. Soc. Jpn. **85**, 053706 (2016).

[24] A. Takemori, S. Miyasaka, S. Tajima, S. Lee, S. Adachi, N. Chikumoto, and K. Tanabe, JPS Conf. Proc. **1**, 012111 (2014).

[25] S. Kimura, T. Ito, M. Sakai, E. Nakamura, N. Kondo, T. Horigome, K. Hayashi, M. Hosaka, M. Katoh, T. Goto, T. Ejima, and K. Soda, Rev. Sci. Instrum. **81**, 053104 (2010).

[26] S. Ishida, M. Nakajima, Y. Tomioka, T. Ito, K. Miyazawa, H. Kito, C. H. Lee, M. Ishikado, S. Shamoto, A. Iyo, H. Eisaki, K. M. Kojima, and S. Uchida, Phys. Rev. B **81**, 094515 (2010).

[27] H. Mukuda, F. Engetsu, T. Shiota, K. T. Lai, M. Yashima, Y. Kitaoka, S. Miyasaka, and S. Tajima, J. Phys. Soc. Jpn. **83**, 083702 (2014).

[28] S. Kitagawa, T. Iye, Y. Nakai, K. Ishida, C. Wang, G.-H. Cao, and Z.-A. Xu, J. Phys. Soc. Jpn. **83**, 023707 (2014).

[29] H. Mukuda, F. Engetsu, K. Yamamoto, K. T. Lai, M. Yashima, Y. Kitaoka, A. Takemori, S. Miyasaka, and S. Tajima, Phys. Rev. B **89**, 064511 (2014).

[30] H. Q. Yuan, F. M. Grosche, M. Deppe, C. Geibel, G. Sparn, and F. Steglich, Science **302**, 2104 (2003).

[31] H. Q. Yuan, F. M. Grosche, M. Deppe, G. Sparn, C. Geibel, and F. Steglich, Phys. Rev. Lett. **96**, 047008 (2006).

[32] G. Seyfarth, A.-S. Ruetschi, K. Sengupta, A. Georges, D. Jaccard, S. Watanabe, and K. Miyake, Phys. Rev. B **85**, 205105 (2012).

[33] S. Watanabe, M. Imada, and K. Miyake, J. Phys. Soc. Jpn. **75**, 043710 (2006).

[34] Y. Zhang, F. Chen, C. He, B. Zhou, B. P. Xie, C. Fang, W. F. Tsai, X. H. Chen, H. Hayashi, J. Jiang, H. Iwasawa, K. Shimada, H. Namatame, M. Taniguchi, J. P. Hu, and D. L. Feng, Phys. Rev. B **83**, 054510 (2011).

[35] Y. Zhang, C. He, Z. R. Ye, J. Jiang, F. Chen, M. Xu, Q. Q. Ge, B. P. Xie, J. Wei, M. Aeschlimann, X. Y. Cui, M. Shi, J. P. Hu, and D. L. Feng, Phys. Rev. B **85**, 085121 (2012).

[36] V. Vildosola, L. Pourovskii, R. Arita, S. Biermann, and A. Georges, Phys. Rev. B **78**, 064518 (2008).

[37] P. Zhang, J. Ma, T. Qian, Y. G. Shi, A. V. Fedorov, J. D. Denlinger, X. X. Wu, J. P. Hu, P. Richard, and H. Ding, Phys. Rev. B **94**, 104517 (2016).

[38] H. Usui and K. Kuroki, Phys. Rev. B **84**, 024505 (2011).

[39] H. Usui, K. Suzuki, K. Kuroki, N. Takeshita, P. M. Shirage, H. Eisaki, and A. Iyo, Phys. Rev. B **87**, 174528 (2013).

[40] H. Usui, K. Suzuki, and K. Kuroki, Sci. Rep. **5**, 11399 (2015).